

In Situ X-Ray Radiographic Study of Intergranular Corrosion in Aluminum Alloys

X. Zhao,* G.S. Frankel,[†]* B. Zoofan,** and S.I. Rokhlin**

ABSTRACT

In situ x-ray radiography was used to characterize intergranular and exfoliation corrosion in high-strength Al alloys. The samples were either exposed to sodium chloride (NaCl) solution at a controlled potential or to high humidity after an electrochemical pretreatment in NaCl solution. Intergranular corrosion (IGC) growth rates in solution for samples encased in epoxy and exposed to solution were distributed over a range with an upper limit equal to the rates determined by the foil penetration technique. Unencased AA2024-T3 (UNS A92024) samples that were held at a controlled potential in solution exhibited IGC and then exfoliation corrosion. AA2024 and AA7178 (UNS A97178) samples encased in epoxy developed sharp intergranular fissures during exposure to 96% RH following an electrochemical pretreatment. Unencased samples given the same treatment exhibited exfoliation in the high-humidity environment.

KEY WORDS: aluminum, exfoliation corrosion, intergranular corrosion, sodium chloride, x-ray radiography

INTRODUCTION

Intergranular corrosion (IGC) and exfoliation corrosion are often found in the high-strength Al alloys (e.g., AA2024 [UNS A92024]⁽¹⁾ and AA7178 [UNS A97178])

used in wingskins and fuselages of airplanes. IGC and exfoliation corrosion are significant sources of life limiting degradation in airframes. A great deal of effort has been devoted over the years to the study of intergranular and exfoliation corrosion of aluminum alloys. The foil penetration technique recently has been used to quantify IGC growth rate.¹ When performed on foils with a range of thickness, foil penetration experiments determine the growth kinetics of the fastest growing localized corrosion sites.²⁻³ However, there are many other sites in such samples that did not penetrate, and those sites had a different set of growth kinetics. It is possible that many sites simply grew slower than the fastest sites. Others might have re-passivated and stopped growing before they penetrated the foil. Still other sites might have started growing after the initiation of the experiment. The latter two types of sites could have had faster growth kinetics than what is determined by the foil penetration technique. It is clearly of interest to obtain information regarding the full population of corrosion sites, not just the sites that penetrate the foil first.

Exfoliation is a form of intergranular corrosion that can occur on the surface of wrought aluminum alloys with elongated grain structure.⁴ However, few reports of quantitative measurements of the kinetics of exfoliation corrosion in Al alloys exist, and little is known about how exfoliation corrosion develops under a wide range of environmental conditions.⁵⁻⁸

Predictive models of the effects of corrosion on the structural integrity of aircraft require information on and prediction of the growth kinetics of the various forms of localized corrosion. X-ray radiography technology is one approach for providing this infor-

Submitted for publication January 2003; in revised form, June 2003.

[†] Corresponding author.

* Fontana Corrosion Center, Department of Materials Science and Engineering, The Ohio State University, Columbus, OH.

** Department of Industrial, Welding, and Systems Engineering, The Ohio State University, Columbus, OH.

⁽¹⁾ UNS numbers are listed in *Metals and Alloys in the Unified Numbering System*, published by the Society of Automotive Engineers (SAE International) and cosponsored by ASTM International.

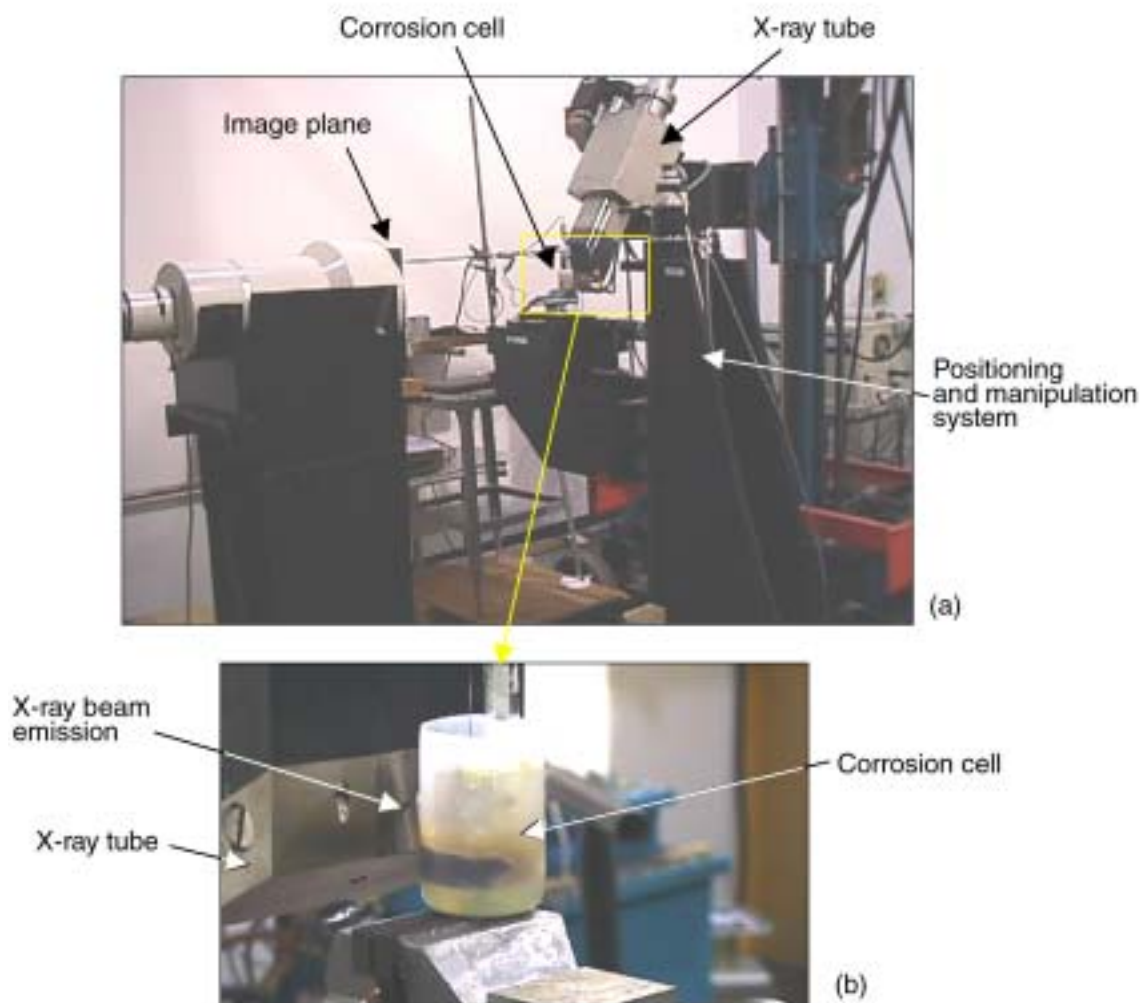


FIGURE 1. (a) Microradiographic imaging system with corrosion cell. (b) Magnified front of x-ray tube and corrosion cell.

mation. The essence of radiography is modulation of the x-ray intensity due to discontinuities or thickness change caused by corrosion.⁹ Owing to the relatively low density of water, x-ray images can be obtained on metal samples in situ, i.e., immersed in solution. Radiography can of course be performed in air as well; so, unlike electrochemical techniques, it can be used on samples exposed to atmospheric conditions, which are more related to the service environment of aircraft components.

In this work, in situ x-ray radiography was used to address localized corrosion kinetics and morphology of AA2024-T3 and AA7178 in different orientations relative to the rolling direction. By orienting the sample properly, based on the understanding generated in prior work, it was possible to image defects growing into a sample.

EXPERIMENTAL PROCEDURES

The microfocal radiographic imaging technique was used in this study. The x-ray source was a

225-kV, 3-mA x-ray unit with 3 μm to 5 μm focal size. The exposure parameters were carefully selected to ensure that the focal spot size remained in the micro-focus region of the tube to get the optimum resolution for each exposure. The position of the sample was controlled by a high-precision positioning system, with three linear (with 2- μm resolution) and one rotation (with 0.01° resolution) computer-controlled axes. One additional high-resolution linear axis was used for translation of the receiver in the image plane. A separate X-Y manipulator was used for positioning of the x-ray source. The microradiographic magnification for this system can be controlled by changing the sample position between the x-ray source and the image plane (the maximum magnification is 300X).

The microradiographic apparatus with corrosion cell is shown in Figure 1. Samples were held with a specially-designed chuck that allowed for precise positioning between the x-ray source and x-ray film holder and accurate repositioning so that intermittent x-ray radiography could be performed on a

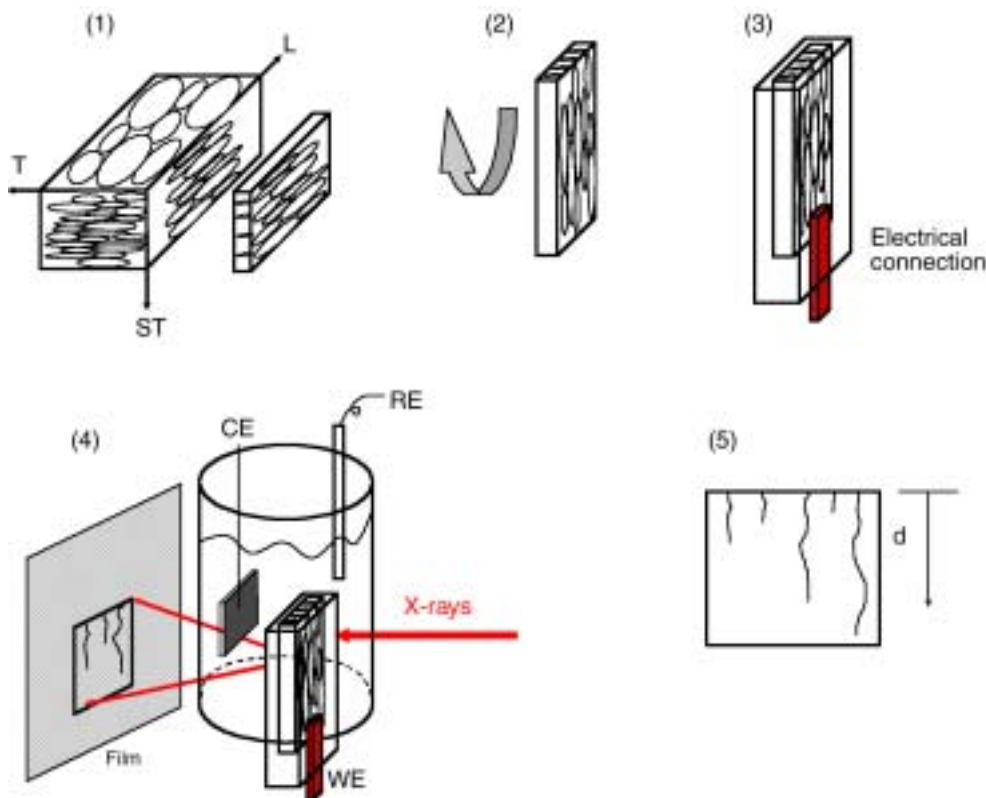


FIGURE 2. Schematic of procedure to make encased sample and in situ radiographic measurement. (1) Cut slice from plate (note nomenclature of orientations); (2) rotate sample; (3) encase sample in epoxy leaving only L face exposed; (4) seal sample in bottom of cell, control potential, and irradiate with x-rays; (5) monitor the number and depth of IGC sites. For study of exfoliation corrosion, the sample is unencased (Step 3 is skipped), and the image shows exfoliation rather than IGC.

sample over an extended period of time. An image intensifier integrated with a charge-coupled device (CCD) camera with a standard frame rate of 30 frames/s was used for the radiographic sample observation in real-time and for alignment of the corrosion cell prior to film microradiography. High-resolution x-ray film was used for higher resolution images; the film was placed in front of the image intensifier for support. The exposed and processed films were digitized by illuminating them in front of a CCD camera. A monochromatic frame grabber board with 2 MB of on-board memory was used for digitization of x-ray films.⁹⁻¹⁰ The sharp images obtained during the microradiography enabled further magnification by the film digitization camera. This optical magnification improved the pixel resolution of the digitized images.

The samples had special configurations relative to the wrought microstructure. Pillars of dimension 30 mm in the longitudinal (L) or rolling direction, 2 mm in the short transverse (S) or through-thickness direction, and 0.8 mm in the long transverse (T) direction were cut from a 19-mm-thick plate of AA2024-T3 (Figure 2). This orientation allowed for IGC or exfoliation corrosion growth in the L direction.

Some samples were oriented such that their longest dimension was along the T direction and the short dimension was along the L direction, allowing the study of IGC or exfoliation corrosion growth in the T direction. Some samples were machined to have a square 2 mm by 2 mm cross section rather than a rectangular section. The samples were positioned with their long dimension vertical and sealed through the bottom of a plastic cell with epoxy.

Some AA2024-T3 samples were encased first in epoxy, except for the top face, which was polished clean. IGC was then generated by polarization in 1 M sodium chloride (NaCl) at a potential of -580 mV vs saturated calomel electrode (SCE) with the sample oriented vertically. The attack was constrained to IGC in the encased samples. Other AA2024-T3 samples were freely exposed to the solution with no epoxy encasement. Freely-exposed samples did not have the physical constraint of the epoxy, and the attack was in the form of exfoliation rather than IGC. These samples had square cross sections with their long axis orientated either in the L or T direction.

IGC and exfoliation corrosion attack (of epoxy-encased and freely-exposed samples, respectively) were studied by in situ x-ray radiography on other

samples during exposure to a high-humidity environment after an initiation pretreatment in chloride solution. These samples were cut from 8.9-mm-thick AA7178 plate removed from the wingskin of a retired KC135 airplane. Samples were machined using a band saw or electric discharge machining (EDM) into long pillars with their long axis orientated in either the L or T direction. Some samples had square cross sections of 2 mm by 2 mm and were exposed freely in the solution to promote exfoliation corrosion. Other samples had cross sections of 0.8 mm by 2 mm and were encased in epoxy leaving only the L face (perpendicular to the L direction) polished and exposed, which promoted IGC rather than exfoliation corrosion. The sample surface was first ground in alcohol to 800 grit. The cell was the same as was used for the AA2024-T3 samples. A 7-h potentiostatic pretreatment in 1 M NaCl was performed to initiate IGC. The applied potential was $-725 \text{ mV}_{\text{SCE}}$ or $-710 \text{ mV}_{\text{SCE}}$ for epoxy-encased or freely-exposed AA7178 samples, respectively. From foil penetration experiments, it is expected that this electrochemical treatment will generate attack $\sim 0.46 \text{ mm}$ deep into the AA7178 samples.¹¹ Following the pretreatment, the samples were rinsed with deionized (DI) water and placed in a sealed desiccator containing saturated sodium sulfate (Na_2SO_4) solution at room temperature. This saturated solution created an environment with constant RH of 96%, as measured by an RH meter. Intermittent x-ray radiography was performed on these samples to obtain information on how IGC and exfoliation corrosion propagated in high humidity.

RESULTS AND DISCUSSION

Before describing the results of the in situ microradiography, an example of metallographic sectioning results will be given. Figure 3 shows an example of a metallographic section for a 3-mm-thick cylindrical AA2024-T3 sample with axial orientation in the S direction after a 4-h exposure at $-580 \text{ mV}_{\text{SCE}}$ in 1 M NaCl. The top and bottom surfaces of the cylindrical sample, the S faces, were coated with epoxy so that the attack was constrained along the L-T plane of the sample (i.e., along the elongated grain boundaries). A series of samples were exposed for different times and sectioned. The kinetics determined from the longest site in each section were slower than those found for L- or T-oriented samples determined by the foil penetration technique, which measures the fastest growing site.¹ This proves that metallographic sectioning does not determine the kinetics of the fastest growing sites.

Figure 4 shows an in situ x-ray microradiograph of a 1-mm-thick AA2024-T3 sample oriented such that the L direction was vertical. The sample was encased in epoxy with one face, the L face, exposed to the solution. This sample was exposed for 19 h to the

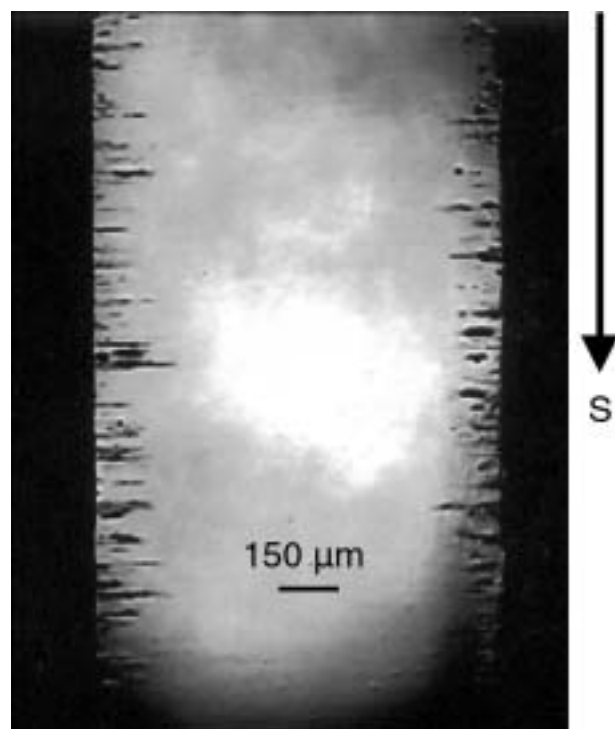


FIGURE 3. Metallographic cross section of S-oriented 3-mm-wide AA2024-T3 cylinder exposed to 1.0 M NaCl at $-580 \text{ mV}_{\text{SCE}}$ for 4 h.

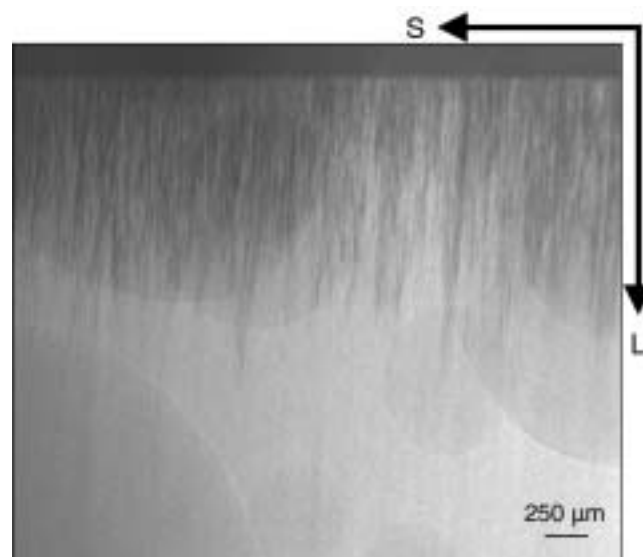


FIGURE 4. In situ x-ray radiograph of L-oriented AA2024-T3 sample exposed to 1.0 M NaCl at $-580 \text{ mV}_{\text{SCE}}$ for 19 h. The dark round features are hydrogen bubbles.

same conditions as the last sample. The dark lines in the image are corroded grain boundaries. Radiographic images of this sample were recorded at varying exposure times, and the depths of specific IG sites are shown as a function of time in Figure 5. The rates comprise a band that falls just beneath the line, representing an extrapolation of the data from

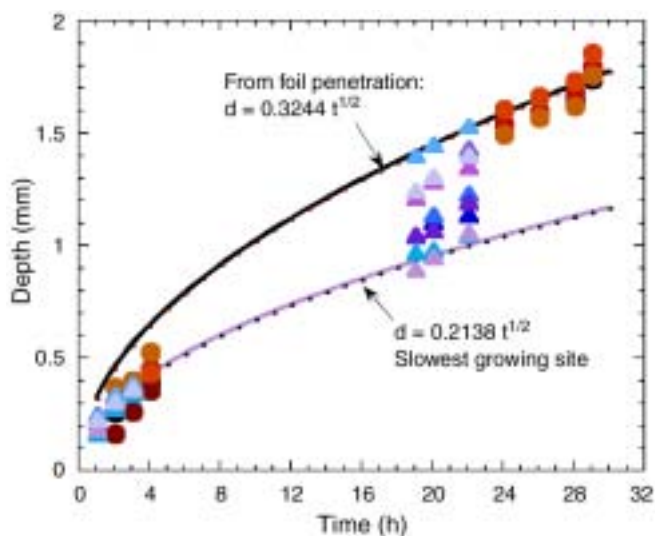


FIGURE 5. Plot of the depth of IGC for L-oriented AA2024-T3 sample as a function of time. The different symbols are for different specific IGC sites in the sample. Also shown is the curve for the L-oriented foil penetration samples.¹

foil penetration experiments.¹ These results show that in situ x-ray radiography provides information on a wide range of growth kinetics, including those for the fastest growing sites.

It should be noted that the circular features in Figure 4 are hydrogen bubbles. Localized corrosion of Al alloys always results in the formation of hydrogen. Aggressive dissolution of the Al alloys for a long period resulted in the formation of a foam in the solution. The low density of the hydrogen bubbles causes them to appear dark, and the bright line along their perimeter is from phase contrast, which highlights the boundary between the bubble and solution.¹²⁻¹⁵

Figure 6 shows radiographs of a similarly oriented sample, with no epoxy encasement, exposed

under the same conditions. This sample had a square 2 by 2 mm cross section. Figure 6(a) shows a radiograph prior to the electrochemical treatment. After 4 h, IGC attack is apparent in the radiographs shown in Figures 6(b) and (c). Since the sample was freestanding with no epoxy encasement, attack proceeded from both the L face on the top and the free T faces on the sides. The period of exposure was too short to generate exfoliation corrosion, so the attack was IGC in nature. However, the IGC propagated inward from three of the five exposed surfaces of the pillar sample: the top L surface and the two side T surfaces. The orthogonal views in Figures 6(b) and (c) show the morphology of attack. In Figure 6(b), the sample is oriented so that the x-rays are parallel to the long transverse direction. IGC can be seen as sharp dark lines. The lines are darker at the top of the sample because the IGC penetrated from the top along the whole thickness. The x-rays integrate the attack throughout the whole thickness of the samples. The fact that the IGC propagated from three faces is clear in Figure 6(c), which is taken at 90° to Figure 6(b), i.e., with the x-rays parallel to the through-thickness or S orientation of the microstructure. The attack is seen to propagate inward from the top L surface and the two side T surfaces. The front of the attack coming from all faces of the sample was evident, and is highlighted in Figure 6(c) by dotted lines. With time, the attack on this freestanding sample developed into exfoliation corrosion. Images of exfoliation corrosion generated after long exposure times on freestanding samples will be given below.

Figure 7(a) shows an in situ x-ray radiograph of a 2-mm-thick AA7178 sample with the long axis oriented in the T direction. The sample was encased in epoxy with one face, the T face, exposed to the solution. This radiograph was taken after 7 h exposure at

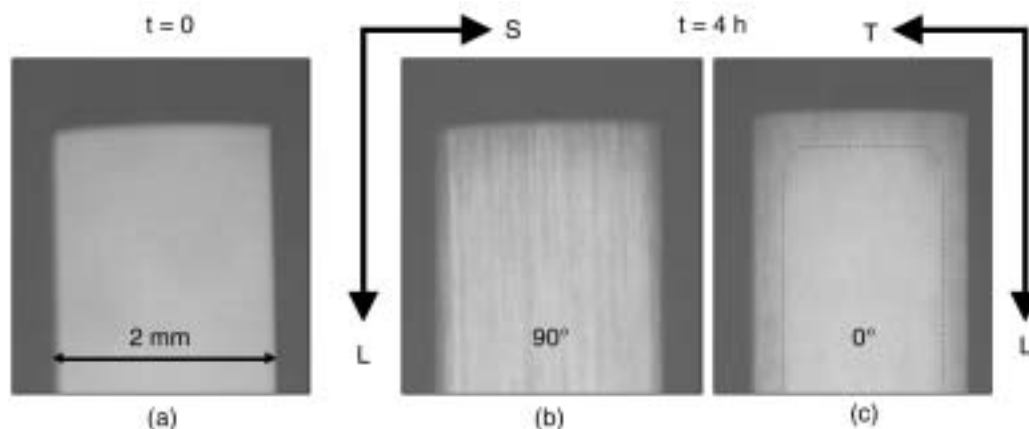


FIGURE 6. Radiographs of a 2-by-2-mm sample of AA2024-T3 exposed to 1.0 M NaCl at $-580 \text{ mV}_{\text{SCE}}$. Sample was not encased in epoxy. Vertical orientation of sample is the L direction. (a) Before exposure; (b) after 4 h exposure, x-rays penetrating in the T direction; and (c) after 4 h exposure, x-rays penetrating in the S direction.

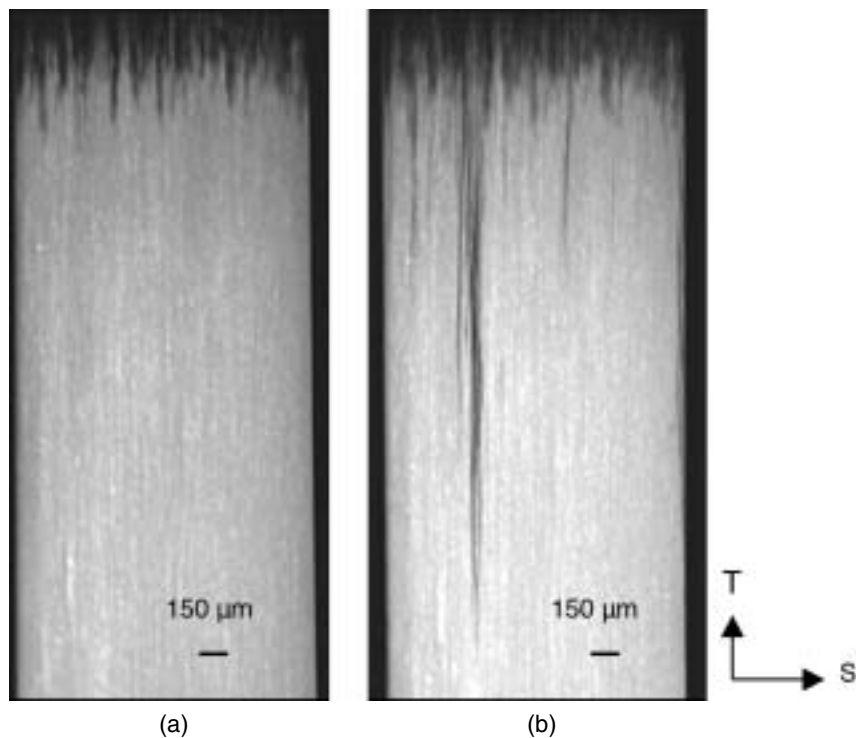


FIGURE 7. Radiographs of AA7178 sample encased in epoxy: (a) immediately after electrochemical pretreatment and (b) after 24 days in 96% RH.

$-725 \text{ mV}_{\text{SCE}}$ in 1 M NaCl. The growth kinetics of selected corrosion sites along the T direction were measured from in situ radiographs during the pretreatment, and it was found that the general law, $d = At^n$, was obeyed for the immersed condition. The value of n was ~ 0.33 and A was 0.23 to 0.34 for values of t in hr and d in mm. This is consistent with results from the foil penetration method.¹¹ After 7 h in 1 M NaCl at $-725 \text{ mV}_{\text{SCE}}$, the sample was rinsed with DI water and placed in 96% RH. Sharp IGC was evident in radiographs after several days of exposure, and it continued to grow at a high rate. Figure 7(b) shows a radiograph of the same sample after 24 days in the high-humidity environment. Tight fissures grew several mm into the sample. Such sharp fissures also can be found in the metallographic cross section for AA2024-T3 samples exposed in the same RH condition. However, it is unclear how these fissures develop and continue to grow at a high rate in the high-humidity environment.

Figure 8 shows x-ray radiographs for a free-standing AA7178 sample. This sample was given the same electrochemical treatment of 7 h in 1 M NaCl at $-710 \text{ mV}_{\text{SCE}}$. The radiographs of the sample taken immediately after this treatment, Figure 8(a), shows IGC, as was found for the freestanding AA2024-T3 sample after short exposure times at a controlled potential. This sample was then exposed to the 96% RH environment for prolonged periods, and exfoliation corrosion rapidly developed, as is evident in Figures

8(b) and (c). These radiographs clearly visualize the exfoliation corrosion and record the progress of the corrosion.

CONCLUSIONS

- ❖ In situ x-ray radiography was used to characterize the intergranular and exfoliation corrosion in high-strength Al alloys exposed to NaCl solution at a controlled potential and to high humidity after an electrochemical pretreatment.
- ❖ Growth kinetics for IGC sites determined from radiographs of samples encased in epoxy and exposed to solution were slower than growth kinetics determined by the foil penetration technique.
- ❖ The unencased AA2024-T3 samples that were exposed to solution exhibited IGC and then exfoliation corrosion.
- ❖ AA2024 and AA7178 samples that were first electrochemically pretreated in chloride solution and then exposed to 96% RH developed sharp intergranular fissures for samples encased in epoxy and exfoliation for unencased samples.

ACKNOWLEDGMENTS

The authors acknowledge the support of AFRL with a contract through S&K Technologies and are grateful to J. Suzel from S&K Technologies for providing the AA7178 samples.

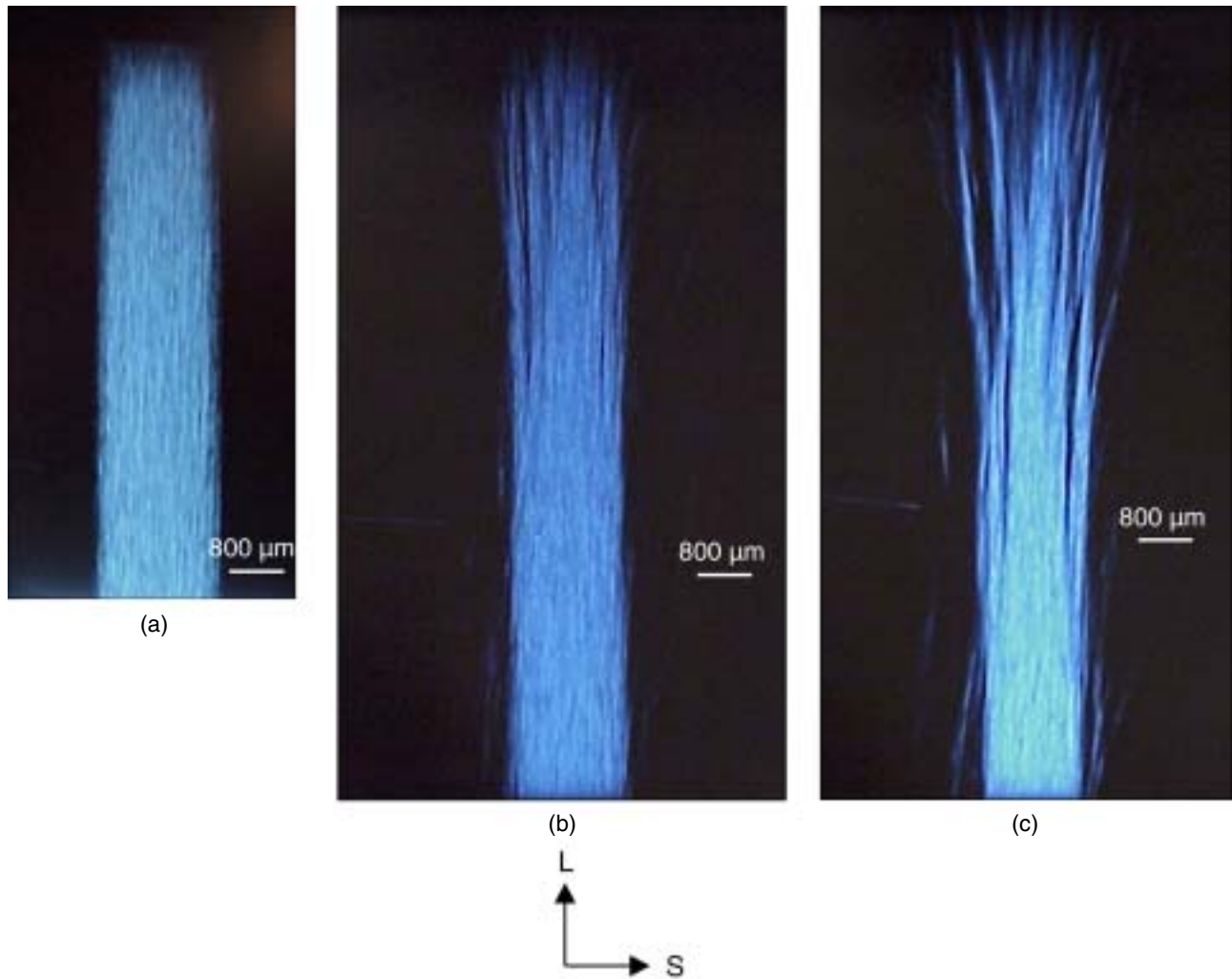


FIGURE 8. Radiographs of AA7178 sample, not encased in epoxy: (a) immediately after electrochemical pretreatment, (b) after 6 days in 96% RH, and (c) after 12 days in 96% RH.

REFERENCES

1. W. Zhang, G.S. Frankel, *Electrochem. Solid-State Lett.* 3, 6 (2000): p. 268-270.
2. F. Hunkeler, H. Bohni, *Corrosion* 37, 11 (1981): p. 645-650.
3. F. Hunkeler, H. Bohni, *Corrosion* 40, 10 (1984): p. 534-540.
4. ASTM STP G34, "Test for Exfoliation Corrosion Susceptibility in 7XXX Series Copper-Containing Aluminium Alloys, EXCO Test," (West Conshohocken, PA: ASTM, 1979).
5. M.J. Robinson, N.C. Jackson, *Corros. Sci.* 41 (1999): p. 1,013-1,028.
6. M.J. Robinson, *Corros. Sci.* 22, 8 (1982): p. 775-790.
7. D.J. Kelly, M.J. Robinson, *Corrosion* 49, 10 (1993): p. 787-795.
8. M.J. Robinson, *Corros. Sci.* 23, 8 (1983): p. 887-899.
9. B. Zoofan, S.I. Rokhlin, *Mater. Eval.* 56, 2 (1998): p. 191-194.
10. A. Sehgal, G.S. Frankel, B. Zoofan, S. Rokhlin, *J. Electrochem. Soc.* 147, 1 (2000): p. 140-148.
11. T.S. Huang, G.S. Frankel, B. Farahbakhsh, D. Peeler, "Localized Corrosion Growth Kinetics in Al Alloys," Proc. of the 6th Joint FAA/DOD/NASA Aging Aircraft Conf. (2002), CD-ROM.
12. T.J. Davis, D. Gao, T.E. Gureyev, A.W. Stevenson, S.W. Wilkins, *Nature* 373, 2 (1995): p. 595-598.
13. S.W. Wilkins, T.E. Gureyev, D. Gao, A. Pogany, A.W. Stevenson, *Nature* 384, 11 (1996): p. 335-338.
14. R. Fitzgerald, *Phys. Today* 7 (2000): p. 23-26.
15. A. Singirev, I. Snigireva, *Rev. Sci. Instrum.* 66, 12 (1995): p. 5,486-5,492.